

■ Coordination Chemistry | *Hot Paper* |



Electronic Consequences of Ligand Substitution at Heterometal Centers in Polyoxovanadium Clusters: Controlling the Redox **Properties through Heterometal Coordination Number**

Rachel L. Meyer, [a] Montaha H. Anjass, *[b, c] Brittney E. Petel, [a] William W. Brennessel, [a] Carsten Streb, *[b, c] and Ellen M. Matson*[a]

Abstract: The rational control of the electrochemical properties of polyoxovanadate-alkoxide clusters is dependent on understanding the influence of various synthetic modifications on the overall redox processes of these systems. In this work, the electronic consequences of ligand substitution at the heteroion in a heterometal-functionalized cluster was examined. The redox properties of [V₅O₆(OCH₃)₁₂FeCl] (1-[V_5 FeCI]) and [V_5O_6 (OCH₃)₁₂Fe]X (2-[V_5 Fe]X; X=CIO₄, OTf) were compared in order to assess the effects of changing the coordination environment around the iron center on the electrochemical properties of the cluster. Coordination of a chloride anion to iron leads to an anodic shift in redox events. Theoretical modelling of the electronic structure of these heterometal-functionalized clusters reveals that differences in the redox profiles of 1-[V₅FeCl] and 2-[V₅Fe]X arise from changes in the number of ligands surrounding the iron center (e.g., 6-coordinate vs. 5-coordinate). Specifically, binding of the chloride to the sixth coordination site appears to change the orbital interaction between the iron and the delocalized electronic structure of the mixed-valent polyoxovanadate core. Tuning the heterometal coordination environment can therefore be used to modulate the redox properties of the whole cluster.

Introduction

Polyoxometalates (POMs) are molecular metal oxide clusters that have shown great utility in many areas of research, including medicinal chemistry,[1] material science,[2] molecular magnetism,^[3] catalysis,^[4] and energy storage.^[5] The rich electrochemical properties and stability exhibited by these polynuclear assemblies make them good candidates for a variety of

[a] R. L. Meyer, B. E. Petel, Dr. W. W. Brennessel, Prof. E. M. Matson Department of Chemistry, University of Rochester Rochester NY 14627 (USA) E-mail: matson@chem.rochester.edu

[b] Dr. M. H. Anjass, Prof. C. Streb Institute of Inorganic Chemistry I Ulm University Albert-Einstein-Allee 11, 89081 Ulm (Germany) E-mail: montaha.anjass@uni-ulm.de carsten.streb@uni-ulm.de

[c] Dr. M. H. Anjass, Prof. C. Streb Helmholtz Institute Ulm (HIU) Helmholtzstrasse 11, 89081 Ulm (Germany)

Supporting information and the ORCID identification number(s) for the author(s) of this article can be found under: https://doi.org/10.1002/chem.201905624.

© 2020 The Authors. Published by Wiley-VCH Verlag GmbH & Co. KGaA. This is an open access article under the terms of the Creative Commons Attribution License, which permits use, distribution and reproduction in any medium, provided the original work is properly cited.

 $[\underline{\hat{\mathbf{Y}}}]_{\hat{\mathbf{C}}}$ Part of a Special Collection to commemorate young and emerging scientists. To view the complete collection, visit: Young Chemists 2020.

electrochemical applications. For example, POMs have displayed great promise as electrocatalysts for the reduction of protons and oxoanions (e.g., nitrite, chlorate, and bromate) and the oxidation of alkanes, alkenes, alcohols, sulfoxides, and phosphines. [6] Recent work has also demonstrated their competency as charge carriers in redox flow batteries.[7]

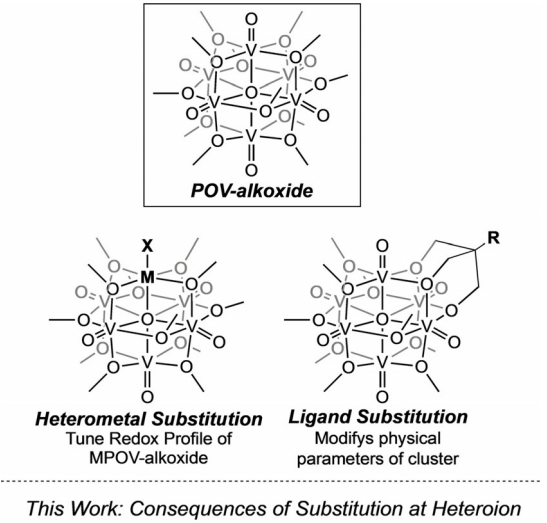
A popular method for modifying the electrochemical properties of polyoxometalates is to incorporate other elements into the cluster framework. For example, in the case of the Keggin polyoxomolybdate cluster $[XMo_{12}O_{40}]^{n-}$ (X = P^V, Si^{IV}, etc.), replacement of the central phosphorus atom with silicon shifts the redox events toward more reducing potentials.[8]

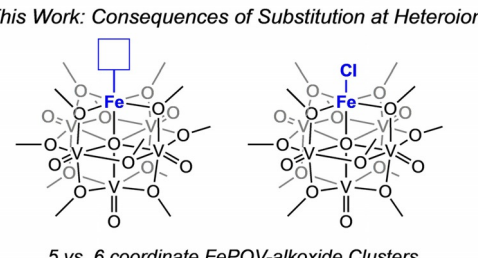
While much is known of strategies to modify the redox properties of molybdate and tungstate clusters, considerably less is understood relating to strategies for modulating the electrochemical profiles of vanadium-oxide derivatives. This is often attributed to the fact that the structural flexibility of vanadium makes precise and controlled modification to polyoxovanadate frameworks challenging. [9] A few examples of functionalized vanadium oxide clusters in the literature illustrate that, like their molybdate and tungstate congeners, the magnetic, photochemical, electrochemical, and catalytic properties of these assemblies can be tuned.[10] However, the development of a general theoretical framework linking systematic molecular modifications to the resulting redox behavior displayed by polyoxovanadates has been outside the scope of these studies.



Toward building a library of polyoxovanadate clusters with tunable physicochemical properties, part of our research team has been studying the synthesis and characterization of Lindqvist polyoxovanadate-alkoxide (POV-alkoxide) clusters, $[V_6O_7(OR)_{12}]$ ($R=CH_3$, C_2H_5). We have demonstrated that the solubility and electrochemical properties of these clusters can be varied through a number of modifications to the cluster core, rendering this family of molecular vanadates useful motifs for probing electrochemical consequences of these structural perturbations (Figure 1). In particular, integration of transition metal or metalloid ions within the cluster core $([V_5O_6(OCH_3)_{12}M]$, $M=Ti^{4+}$, Zr^{4+} , Hf^{4+} , Fe^{3+} , Ga^{3+}) has been shown to serve as an effective method for tuning the redox properties of POV-alkoxides, $I^{12}I^{12}$ similar to previous studies on heterometallic tungstates and molybdates.

While we have provided extensive evidence that the aforementioned variations of heteroion and bridging alkoxide ligand identity can modify the physicochemical properties of the assembly, the effects of modifying the ligand environment surrounding a heteroion embedded within a POV cluster have not been reported. This gap of knowledge is striking when considering the importance of ligand field considerations in dictating the electronic structure of monometallic, transition metal complexes. Herein, we report the electrochemical consequences of halide coordination to the heterometal of an ironfunctionalized POV-alkoxide cluster, [V₅O₆(OCH₃)₁₂FeCl], and comparing its redox properties to that of previously reported, iron-installed POV-alkoxide clusters (Figure 1). A combination





5 vs. 6 coordinate FePOV-alkoxide Clusters Consequences of Ligand Substitution at Heterometal on Redox Properties of FePOV-alkoxide Clusters

Figure 1. Previously reported synthetic modifications for POV-alkoxide clusters. [7,13]

www.chemeuri.org

of experimental and theoretical investigations is used to develop a more complete understanding of the comparative electrochemical effects of incorporating coordinating (e.g., chloride) versus non-coordinating (e.g., perchlorate) ligands at the site-differentiated metal center.

Results and Discussion

Electrochemical characterization of 1-[V₅FeCl]

The isolation of the chloride-functionalized analogue of the iron-containing species, $[V_5O_6(OCH_3)_{12}FeCl]$ (1- $[V_5FeCl]$), was previously reported by some of us, using an adapted synthetic procedure to that reported for the gallium-functionalized variant, $[V_5O_6(OCH_3)_{12}GaCl]$. [12d] Briefly, self-assembly of the heterometallic Lindqvist cluster occurs following heating of a tetrahydrofuran solution of $[VO(OCH_3)_3]$ (5 equiv.) and $FeCl_3$ (2 equiv.) in the presence of NaBH₄ (1 equiv.). Spectroscopic investiga-

Carsten Streb is Director of the Institute of Inorganic Chemistry I at Ulm University and group leader at the Helmholtz Institute Ulm. His love for POMs started during his PhD, working with Lee Cronin at the University of Glasgow. His current research is focused on designing POM-based functional materials and composites to address global chemical challenges including energy conversion/storage, water purification and public health. In particular, he enjoys exploring the supramolecular chemistry and metal-functionalization of molecular vanadium oxide clusters.



Montaha Anjass is independent research group leader and Margarete-von-Wrangell-Fellow at Ulm University and Helmholtz Institute Ulm. She received her B.Sc. degree in Chemistry from Birzeit University, Palestine and her M.Sc. degree in Advanced Materials from Ulm University, Germany. In 2019, she completed her PhD (supervisors: C. Streb, M. Fichtner, T. Jacob) at Ulm University. From 2019–2020 she undertook a postdoc at Helmholtz-Institute Ulm. Her current research interests are advanced battery materials based on redox-active molecular metal oxides and electrically conductive organic polymers and their use in (post-)lithium batteries.



Ellen Matson received her PhD from Purdue University. Following a postdoctoral appointment at the University of Illinois at Urbana-Champaign, Matson began her independent career at the University of Rochester (2015), where she is currently the Wilmot Assistant Professor of Chemistry. The Matson Laboratory studies the synthesis and reactivity of reduced vanadium oxide clusters. Ellen Matson has earned several awards recognizing early success in research and teaching, including a Sloan Fellowship, a Cottrell Scholar Award, a Camille Dreyfus Teaching-Scholar Award and the Edith Flanigen Award.





tions and charge balancing revealed the oxidation state distribution for complex 1-[V_5 FeCI] to be $V^{IV}_3V^V_2$ Fe^{III}. While the electronic structure of the neutral species was rigorously characterized, the electrochemical profile of 1-[V_5 FeCI] was not explored. Thus, we set out to understand the consequences of halide-coordination to the heteroion in 1-[V_5 FeCI] on its redox chemistry and electronic structure.

The cyclic voltammogram (CV) of 1-[V₅FeCl], collected in acetonitrile, displayed four, evenly spaced redox events (E_{1/2}= -0.68, -0.21, +0.31, +0.83 V vs. Fc^{0/+}; Figure 2); CV experiment with expanded electrochemical window can be found in Figure S1 in the Supporting Information. These events are anodically shifted compared to the hexavanadate cluster by approximately 0.1 V. Thus, the replacement of a "V=O" unit for a "Fe-CI" effectively modulates the potentials of the redox processes without compromising the rich electrochemical properties. This modulation has also been observed in other heterometal-functionalized POV-alkoxides. [12c,d] Interestingly, comparing the redox profile of 1-[V₅FeCl] to other iron-functionalized POV-alkoxide clusters reported by our group, namely $[V_5O_6(OCH_3)_{12}Fe]X$ $(X = CIO_4, 2-[V_5Fe]CIO_4; X = OTf,$ [V₅Fe]OTf), shows that the series of four electrochemical events of the halogenated species is shifted by approximately 1 V. This substantial anodic shift upon coordination of the chloride is unexpected, as the additional negative charge supplied by the anionic ligand should shift the redox profile to more reducing potentials. As such, a more in-depth chemical analysis of the electronic characteristics of 1-[V₅FeCl] is required to explain this result.

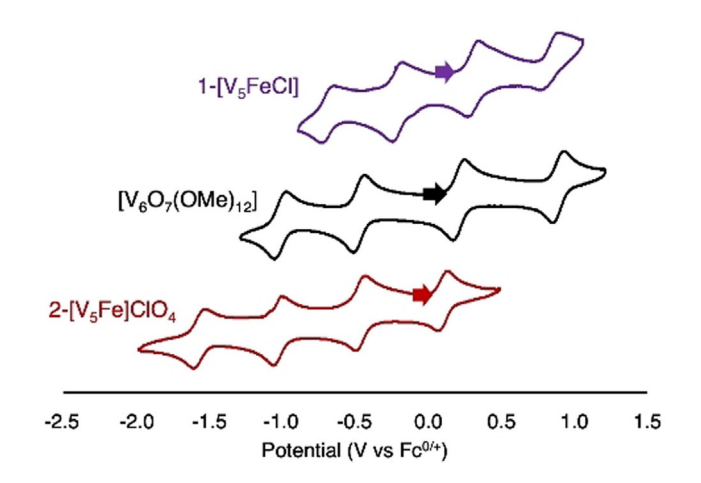


Figure 2. Cyclic voltammograms of **1-[V₅FeCl**] (Purple), $[V_6O_7(OCH_3)_{12}]$ (Black), and **2-[V₅Fe]ClO₄** (Red) collected in acetonitrile (0.1 $\,$ M $[nBu_4N][PF_6]$ as supporting electrolyte, referenced to $Fc^{0'+}$).

Isolation of redox isomers of 1-[V₅FeCl]

The striking differences in the electrochemical profiles of the two FePOV-alkoxide clusters, $1-[V_5FeCI]$ and $2-[V_5Fe]X$ (X = CIO₄, OTf), prompted a detailed investigation to understand the changes in the electronic structure of $1-[V_5FeCI]$ across all charge states. We hypothesized that the change in coordina-

www.chemeurj.org

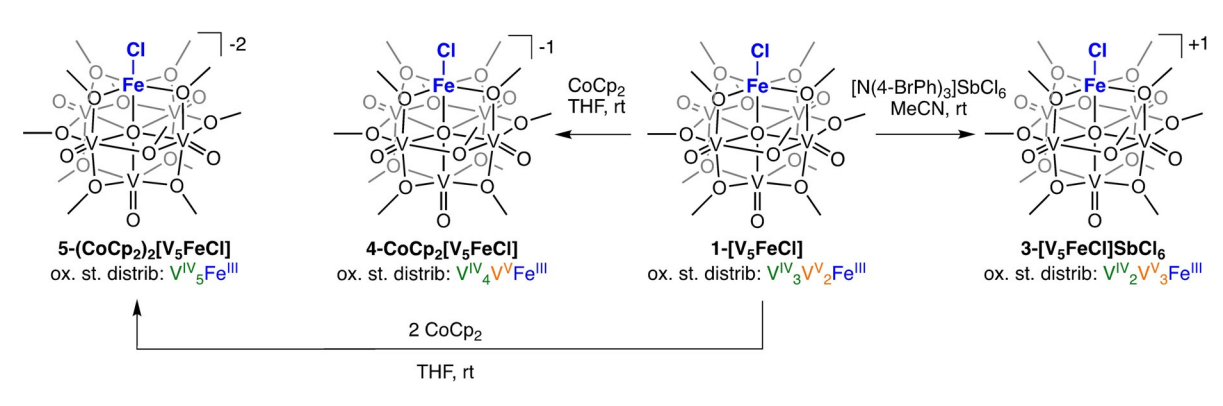
tion number of the iron center might be influencing the energetics of electron storage and release in these heterometallic assemblies. Indeed, the neutral complex $1-[V_5FeCl]$ has been shown to retain a 6-coordinate iron center (pseudo O_h geometry) in the solid-state and in solution. [12d] In contrast, we have previously reported that the coordination environment of iron in complex $2-[V_5Fe]X$ (X = OTf, CIO_4) is best described as square pyramidal (5-coordinate), as the weakly-coordinating nature of OTf⁻ and ClO₄⁻ counter ions results in their dissociation from the cluster core. [12a,b] These conclusions are supported by Mössbauer analysis of solid-state samples, revealing a mixture of the 5-coordinate (62%) and 6-coordinate (38%) species in complex 2-[V5Fe]X. Following cluster reduction, the mixture collapses to a single set of resonances consistent with a 5-coordinate Fe^{III}. Electrospray ionization-mass spectrometry (ESI-MS) data also suggests that, in solution, the counter ion $(X = OTf, CIO_4)$ is fully dissociated from the iron-functionalized POV-alkoxide core.

To establish whether the cathodic shift in the redox profile of $1-[V_5FeCl]$ relative to $2-[V_5Fe]X$ is a general phenomenon for iron-functionalized POV-alkoxide clusters containing 6-cooridnate iron centers, we obtained the CV of the previously reported complex $[V_5O_6(OCH_3)_{12}Fe(OCN)]$, $1-[V_5FeOCN]$ in acetonitrile (Figure S2, Table S1, CV experiment with expanded electrochemical window in Figure S3). The cyanate derivative was selected because the cyanate anion has been shown to strongly bind to the iron center, and thus is a good example of a 6-coordinate species. The CV of the cyanate-functionalized cluster is identical to that of $1-[V_5FeCl]$, providing further support for our hypothesis that the observed ligand-dependent shifts in redox potentials result from changes in coordination number of the iron center, rather than ligand identity.

In particular, we became interested in understanding how the coordination of a chloride ion to the heterometal (iron) affects the storage and release of electron density from the cluster. Synthetic isolation of the various oxidation states of **2**- $[V_5Fe]ClO_4$ and $[V_6O_7(OR)_{12}]$ ($R=CH_3$, C_2H_5) has been shown to be an effective method at elucidating the electrochemical properties of these heterometallic systems. [11b,c,12b] As such, we sought to perform a similar analysis with **1-[V_5FeCl]**.

In our original report of the synthesis of **1-[V₅FeCl]**, we proposed that the FePOV-alkoxide cluster bears a mixed-valent oxidation state distribution of metal ions $(V_2^V V_3^V Fe^{III})$. The open circuit potential of the neutral cluster $(-0.05 \text{ V vs. Fc}^{0/+})$ is located between sets of two reduction and oxidation waves. This suggests that the parent cluster **1-[V₅FeCl]** could be twice oxidized and twice reduced, affording a family of five redox isomers of the FePOV-alkoxide cluster, each differing by a single electron.

Toward isolating the redox series of iron-functionalized POV-alkoxide clusters, outlined in Scheme 1, we first set out to synthesize the two products of oxidation. The mono-cationic cluster, $[V_5O_6(OCH_3)_{12}FeCl]OTf$ (3- $[V_5FeCl]OTf$), has been previously isolated by addition of a sub-stoichiometric amount of WCl₆ to 2- $[V_5Fe]OTf$. To independently synthesize the mono-cationic species from the iron-chloride functionalized POV-alkoxide cluster, an equivalent of $(N(C_6H_4Br-4)_3)SbCl_6$ ($E^0=0.67$ V vs. $Fc^{0/2}$)



Scheme 1. Synthesis and proposed structures of redox isomers of $1-[V_5FeCI]$. Synthesis of complexes $3-[V_5FeCI]SbCI_6$, $4-CoCp_2[V_5FeCI]$, and $5-(CoCp_2)_2[V_5FeCI]$.

⁺ in acetonitrile)^[13] was added to **1-[V₅FeCl**] in acetonitrile. The ¹H NMR spectrum of the product, [V₅O₆(OCH₃)₁₂FeCl]SbCl₆ (**3**-[V₅FeCl]SbCl₆), in CD₃CN revealed two paramagnetic resonances at 14.5 (24H) ppm and 12.5 (12H) ppm (Figure S4). Based on the pseudo-C_{4V} symmetry of the cluster, one would expect three resonances in the ¹H NMR spectrum of 3-[V₅FeCI]SbCl₆. However, a two-peak pattern with broad resonances that possess a 2:1 ratio suggests that two sets of chemically equivalent methoxide ligands overlap in this spectrum. Similar patterns to those observed in the ¹H NMR spectrum of 3-[V₅FeCl]SbCl₆ have likewise been reported for other iron-functionalized, POValkoxide clusters. [12a,b] These signals are substantially shifted from those of the starting material (δ = 23.3 ppm and 13.3 ppm), suggesting complete conversion to the desired oxidized cluster. Furthermore, the ¹H NMR spectrum of 3-[V₅FeCI]SbCl₆ collected in [D₈]THF matches that of previously reported **3-[V₅FeCl]OTf** (Figure S5). The product composition was further confirmed by elemental analysis and ESI-MS (Figure S6).

The CV of complex 1-[V₅FeCl] suggests a second, more-oxidized product should be accessible via the two-electron oxidation of the parent cluster. However, addition of two equivalents of NOPF₆ to 1-[V₅FeCl] in dichloromethane (NOPF₆ in dichloromethane, $E^0 = 1.00 \text{ V}$ vs. $Fc^{0/+})^{[13]}$ resulted in the formation of the mono-cationic species, [V₅O₆(OCH₃)₁₂FeCl]PF₆ (confirmed by ¹H NMR and infrared spectroscopic analyses, Figure S7). Attempts to electrochemically access the di-cationic species, via bulk oxidation in acetonitrile, resulted in decomposition (Figure S8). Indeed, the poor chemical reversibility of this second oxidation event is illustrated when the redox process is isolated at varying scan rates from 10 to 1000 mV s⁻¹ in acetonitrile (Figure S9). As the scan rate is increased, the peak-topeak separation between the oxidative and reductive features increases and the redox event becomes ill defined. These results suggest that the most oxidizing event is actually an irreversible process. The inability to synthetically or electrochemically access the di-cationic species of 1-[V₅FeCl] is not wholly surprising, as we have previously reported the oxidative instability of the homometallic POV-alkoxide cluster, $[V_6O_7(OCH_3)_{12}].^{[7d,\,11a]}$

In principle, the $E_{1/2}$ value of the most oxidizing event of complex 1-[V₅FeCl] occurs at a potential at which chloride oxidation is possible. To assess whether the irreversibility of this redox event was due to chloride dissociation and subsequent oxidation, we titrated a solution of (nBu₄N)Cl into a CV cell containing 1-[V₅FeCl] (see supporting information for experimental details, Figure S10). Heterogeneous chloride oxidation results in a distinct electrochemical event at a potential of 0.79 V (vs. Fc^{0/+}), as indicated by an increased current response proportional to increased concentrations of (nBu₄N)Cl in the first scan rate of the sample. Third scan analysis, allowing for the sample to reach chemical equilibrium, reveals chloride consumption, and retention of the four redox processes native to complex **1-[V₅FeCl]** (Figure S10), indicating that Cl₂ production does not correlate with cluster decomposition. As such, we hypothesize that the observed lack of reversibility is indicative of complete cluster degradation, and not dissociation/oxidation of the chloride ligand.

To access the two reduced forms of complex $1-[V_5FeCI]$ observed by CV, stoichiometric reductions of the neutral FePOV-alkoxide cluster were performed. Previously, we have reported isolation of a series of reduced, FePOV-alkoxide clusters resulting from addition of various equivalents of potassium graphite (KC₈) to $2-[V_5Fe]CIO_4$. To mirror these synthetic procedures, one or two equivalents of KC₈ were added to $1-[V_5FeCI]$. In the case of the mono-reduced derivative, the desired product, K[V₅O₆(OCH₃)₁₂FeCI] (4-K[V₅FeCI]), was isolated in good yield (87%). Formation of 4-K[V₅FeCI] was verified by 1 H NMR spectroscopy (23.8 (24H) and 18.1 (12H) ppm; Figure S11), ESI-MS (Figure S12), and elemental analysis.

While the reduction of $1-[V_5FeCI]$ with one equivalent of KC_8 cleanly afforded the mono-reduced cluster, attempts to isolate the di-reduced species proved challenging. Addition of two equivalents of KC_8 to $1-[V_5FeCI]$ resulted in the removal of the chloride ion, as confirmed by 1H NMR and infrared spectroscopies (Figure S13). The spectra of the crude reaction compares favorably to that previously reported for the monoanionic, iron-functionalized POV-alkoxide cluster, $K[V_5O_6(OCH_3)_{12}Fe]$. We hypothesized that the removal of the chloride ion from the surface of the cluster is promoted by the preferential formation of potassium chloride under highly re-



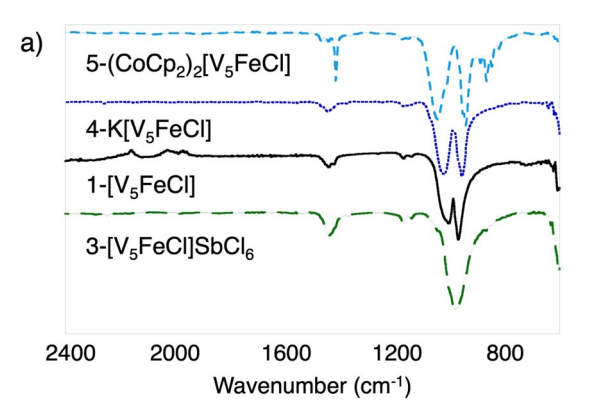
ducing conditions. Thus, we opted to use a non-coordinating reductant with an appropriate redox potential to isolate the direduced species. Gratifyingly, the addition of two equivalents of cobaltocene (CoCp $_2$, $E^0\!=\!-1.33~V$ vs. $Fc^{0/+}$ in acetonitrile) to 1-[V₅FeCI] afforded the fully-reduced, heterometallic Lindqvist cluster, $(CoCp_2)_2[V_5O_6(OCH_3)_{12}FeCI]$ (5-(CoCp₂)₂[V₅FeCI]), in good yield (42%), as confirmed by ¹H NMR spectroscopy (Figure S14, δ = 24.1 and 22.1 ppm)), ESI-MS (Figure S15), and elemental analysis. Retention of the chloride-bound, iron-functionalized, Lindqvist formulation upon reduction to 5-(CoCp₂)₂[V5FeCl] was unambiguously confirmed through single crystal X-ray structural analysis (Figure S16; Table S2). The cobaltocenium derivative of the mono-reduced cluster, CoCp₂[V₅O₆(OCH₃)₁₂FeCl] (**4-CoCp₂[V₅FeC**]), could also be isolated by reacting one equivalent of CoCp₂ with 1-[V₅FeCl]. Characterization of **4-CoCp₂[V₅FeCI]** via ¹H NMR (Figure S17) spectroscopy and ESI-MS (Figure S18) matches that of 4-K[V₅FeCI]. Furthermore, structural analysis of the mono-reduced species, **4-CoCp**₂[**V**₅FeCl], *via* single-crystal X-ray diffraction revealed the expected halide-functionalized Lindqvist structure (Figure S19, Table S2).

Electronic structure of the redox isomers of 1-[V₅FeCl]

With the oxidized and reduced clusters in hand, we turned to elucidating the electronic characteristics of these compounds. In particular, we were interested in understanding the participation of transition metal ions in the reduction and oxidation events observed in the CV of complex $1-[V_5FeCI]$. Fourier-transform infrared (FT-IR) and electronic absorption spectroscopies are complementary techniques that have been used to give valuable insight into the oxidation state distribution within POV-alkoxide clusters. [11b,c,12b] Thus, we applied these spectroscopic methods to analyze the electronic structures of $1-[V_5FeCI]$, $3-[V_5FeCI]SbCI_6$, $4-K[V_5FeCI]$, and $5-(CoCp_2)_2[V_5FeCI]$.

The FT-IR spectra of $1-[V_5FeCI]$, $4-K[V_5FeCI]$, and $5-(CoCp_2)_2[V_5FeCI]$ (Figure 3a, Table S3) display two intense bands located at $941-969~\text{cm}^{-1}$ and $1043-1003~\text{cm}^{-1}$, corresponding to the terminal oxido, $v(V=O_t)$, and the bridging methoxide, $v(O_b-CH_3)$, vibrations, respectively. The presence of a singular $v(V=O_t)$ and $v(O_b-CCH_3)$ band in the FT-IR spectra of POV-alkoxide clusters is characteristic of the Robin and Day Class II delocalized electronic structure displayed by these assemblies. Therefore, the FT-IR spectra of the $1-[V_5FeCI]$ redox series show that both the Lindqvist motif and the electronic delocalization are retained as electrons are added and removed.

As the cluster is oxidized from the di-anionic to the neutral species, the $v(V=O_t)$ band shifts to higher energy. This is consistent with the strengthening of the terminal V–O bond as electron density is removed from the cluster core. In contrast, the $v(O_b\text{-CH}_3)$ band shifts to lower energy upon oxidation as a result of the decrease in the partial negative charge on the bridging oxygen atoms. The FT-IR spectrum of $3\text{-[V}_5\text{FeCI]SbCI}_6$ only displays one broad band at 984 cm⁻¹, which is due to the $v(V=O_t)$ and $v(O_b\text{-CH}_3)$ vibrations shifting upon oxidation such



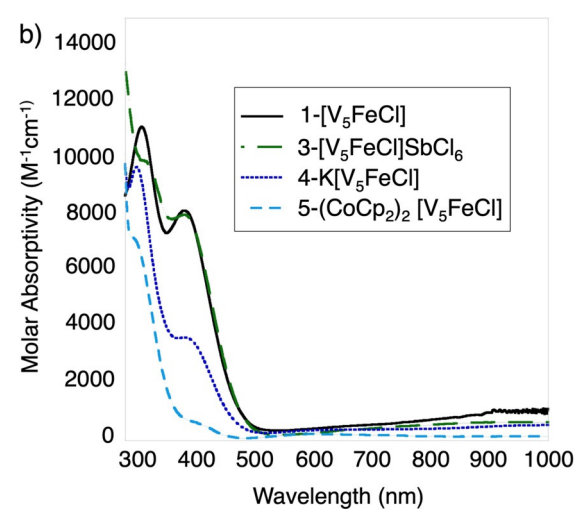


Figure 3. a) infrared spectra and b) electronic absorption spectra (collected in acetonitrile) of 1-[V_s FeCI], 3-[V_s FeCI]SbCI₆, 4-K[V_s FeCI], and 5-(CoCp₂)₂[V_s FeCI].

that they overlap. Similar shifts in the $v(V=O_t)$ and $v(O_b\text{-OCH}_3)$ bands upon oxidation have been observed in other iron-functionalized, POV-alkoxide clusters. For these systems, the redox activity was shown to be localized on the vanadium centers, while the Fe^{III} center did not show any redox-activity across the redox series. The chloride-functionalized derivatives reported here appear to behave in a similar manner.

Next, electronic absorption spectra of the redox isomers of the halide-functionalized clusters were collected in acetonitrile (Figure 3b, Table S4). Complexes 1-[V₅FeCI], 3-[V₅FeCI]SbCI₆, and 4-K[V₅FeCI] all have absorbance features at 382 and 990 nm, diagnostic of mixed valent (VIV/VV), POV-alkoxide clusters. The higher energy feature corresponds to the $V^{IV}(d_{xy}) \rightarrow$ $V^{V}(d_{x2-y2})$ intervalence charge transfer (IVCT), while the lower energy is assigned to a $V^{IV}(d_{xy}) \rightarrow V^{V}(d_{xy})$ IVCT event. [11c, 12a, d] The intensity of the electronic transitions between V^{IV} and V^V centers vary with the number of V^{IV} and V^{V} within the clusters, thus giving insight into the oxidation state distribution of the metal centers. For example, if the reduction of 1-[V₅FeCl] to 4-K[V₅FeCl] is vanadium-based, the molar absorptivity of the two IVCT bands should be halved, as the number of VV ions decreases from two to one; we note that this prediction is observed. Furthermore, the absorbances of the 382 and the 990 nm bands of the 3-[V₅FeCl]SbCl₆ are similar to those of 1-



 $\mbox{[$V_5$FeCl]}.$ This is consistent with $\mbox{V''}_3\mbox{V'}_2\mbox{Fe}^{III}$ and $\mbox{V''}_2\mbox{V''}_3\mbox{Fe}^{III}$ assignments for 1-[V₅FeCl] and 3-[V₅FeCl]SbCl₆, respectively, as there are two pairs of V^{IV} and V^{V} ions for charge transfer to occur in both clusters.

In the case of complex 5-(CoCp₂)₂[V₅FeCl], the absence of the characteristic $V^{IV} \rightarrow V^{V}$ IVCT in the electronic absorption spectrum indicates an isovalent oxidation state distribution of vanadium ions within the cluster, that is, [V^{IV}₅Fe^{III}]. In line with this oxidation state assignment, a low intensity absorption feature at 598 nm (235 cm⁻¹ м⁻¹) is observed. Similar absorption features have been observed in other hexavanadate and heterometallic POV-alkoxides, where all the vanadium ions are in the tetravalent state, and has been assigned as a transition localized on a single V^{IV} center. $^{\text{[11b,c,12b,c]}}$

An additional intense feature between 294 and 316 nm is observed for all redox isomers. In our previous work with heterometal-functionalized POV-alkoxide clusters bearing a chloride ligand (1-[V₅FeCl] and [V₅O₆(OCH₃)₁₂TiCl]), this has been assigned as a CI:→M ligand-to-metal charge transfer (LMCT) event. [12d,14] The presence of this feature in each redox isomer confirms that the chloride ion remains bound to the cluster in solution. Notably, as the halide-functionalized FePOV clusters are reduced, a hypsochromic shift in the CI:→Fe^{III} transition occurs. This implies that while the redox activity of 1-[V₅FeCl] is localized to the vanadium ions, the surrounding POV-alkoxide framework affects the electronic structure of the Fe-Cl moiety. Specifically, as the metalloligand becomes more electron rich, the ability of the Fe^{III} center to accept electron density from the chloride anion decreases. While oxygen-to-vanadium LMCT bands might also occur in these high-energy regimes, the absence of these bands in the spectra of POV-alkoxide clusters lacking halide ligands suggests that this feature indeed derives from an electronic transition from CI to the heteroion (Figure S20).

Taken together, the spectroscopic data of complexes 1-[V_5FeCI], 3-[V_5FeCI]SbCI₆, 4-K[V_5FeCI], and 5-($CoCp_2$)₂[V_5FeCI], confirm that the redox activity of the cluster is localized within the vanadate cluster core. This is consistent with our previous reports investigating the redox chemistry of heterometal-functionalized POV-alkoxide clusters. [12b-d] We can thus assign the oxidation states distributions of transition metal ions in the chloride-functionalized, iron-functionalized POV clusters as follows: $5-(CoCp)_2[V_5FeCI] = [V^{IV}_5Fe^{III}]$, $4-K[V_5FeCI] = [V^{IV}_4V^VFe^{III}]$, $1-V^{IV}_5Fe^{III}$ $[V_5FeCI] = [V_3^{V_3}V_2^{V_3}Fe^{III}]$, and $3-[V_5FeCI]SbCI_6 = [V_2^{V_2}V_3^{V_3}Fe^{III}]$. These assignments allow for a more appropriate comparison of the electronic structures of complex 1-[V_5 FeCI] and 2-[V_5 FeX] (X = OTf, CIO₄) (vide infra).

Theoretical analysis of the electrochemical properties of 1-[V₅FeCl] versus 2-[V₅Fe]ClO₄

With the oxidation state distributions for the redox isomers of 1-[V₅FeCl] identified, we became interested in gaining a fundamental understanding of how the coordination environment around the iron center imparts the different electrochemical behaviors observed in the CV of 1-[V₅FeCl] and 2-[V₅Fe]ClO₄. As such, theoretical calculations were employed. First, the redox transitions of 1-[V_5 FeCI] (CN=6) and 2-[V_5 Fe]CIO₄ (CN= 5) were obtained by DFT-level calculations using the B3LYP functional via the Jaguar program suite (see SI for details).[15] As shown in Table 1, the theoretically calculated reduction potentials for processes 1', 2', and 3' for 1-[V₅FeCl] are in excellent agreement with the experimentally observed values, with maximum deviations < 0.1 V. However, for process 4', the experimental data (-0.68 V) differs significantly from our calculated value (-0.37 V). This is possibly related to solvation effects, where the acetonitrile solvation shell surrounding 1-[V₅FeCl] is bound rather strongly as the negative charge is increased. [8] For 2-[V₅Fe]ClO₄, where we expect dissociation of the perchlorate ion in solution, the calculations were performed for the 5coordinate iron center. The reduction potentials for the experimentally observed processes 2', 3', and 4' are in excellent agreement with the calculated values, with maximum deviations < 0.1 V. However, for process 5', we note a significant difference in calculated and experimental reduction potentials (ΔE ca. 1.7 V). This deviation is currently not understood and still under investigation. We hypothesize that it might be related to changes of the coordination environment around the iron center upon accessing the di-anionic species.

Frontier molecular orbital analysis of the highest occupied molecular orbitals (HOMO) of all five possible redox isomers observed in the CV of 1-[V₅FeCl] (Figure 4) indicate that all reduction processes 1', 2', 3', and 4' lead to the reduction of the vanadium centers in 1-[V₅FeCl]. This results in a retention of the ferric center throughout the series of redox isomers. Similar observations were made upon analysis of complex 2-[V₅Fe]ClO₄ (Figure S21), where the calculation showed the redox activity to be localized to the POV scaffold. Furthermore, the atomic spin densities from Mulliken analysis for the complete set of redox-isomers for both clusters shows that iron center remains as high-spin iron(III) ion $S_{Fe} = \frac{5}{2}$ (Table S5, S6). These assignments are consistent with the experimental results described above.

With the validity of these calculations established, the individual redox profiles of 1-[V₅FeCl] and 2-[V₅Fe]ClO₄ were analyzed theoretically by DFT-level computations to gain insights

Table 1. Experimental and calculated reduction potentials for 1-[V₅FeCl] and 2-[V₅Fe]ClO₄. All potentials referenced against Fc ^{0/+} .										
Redox process	$V^{IV}V^{V}_{4}Fe^{III}/V^{IV}_{2}V^{V}_{3}Fe^{III}$		$V_{2}^{IV}V_{3}^{V}Fe^{III}/V_{3}^{IV}V_{2}^{V}Fe^{III}$		$V^{IV}_{3}V^{V}_{2}Fe^{III}/V^{IV}_{4}V^{V}Fe^{III}$		$V^{IV}_{4}V^VFe^{III}/V^{IV}_{5}Fe^{III}$		V ^{IV} ₅ Fe ^{III} /V ^{III} V ^{IV} ₄ Fe ^{III}	
Step Number 1-[V ₅ FeCl] (CN = 6) 2-[V ₅ Fe]ClO ₄ (CN = 5)	1' E _{exp.} /V 0.83	E _{calcd} /V 0.83	2' E _{exp.} /V 0.31 0.21	E _{calcd} /V 0.34 0.21	3' E _{exp.} /V -0.21 -0.36	E _{calcd} /V -0.28 -0.33	4' E _{exp.} /V -0.68 -0.94	E _{calcd} /V -0.37 -0.85	5' E _{exp.} /V1.46	E _{calcd} /V — —3.23

www.chemeurj.org

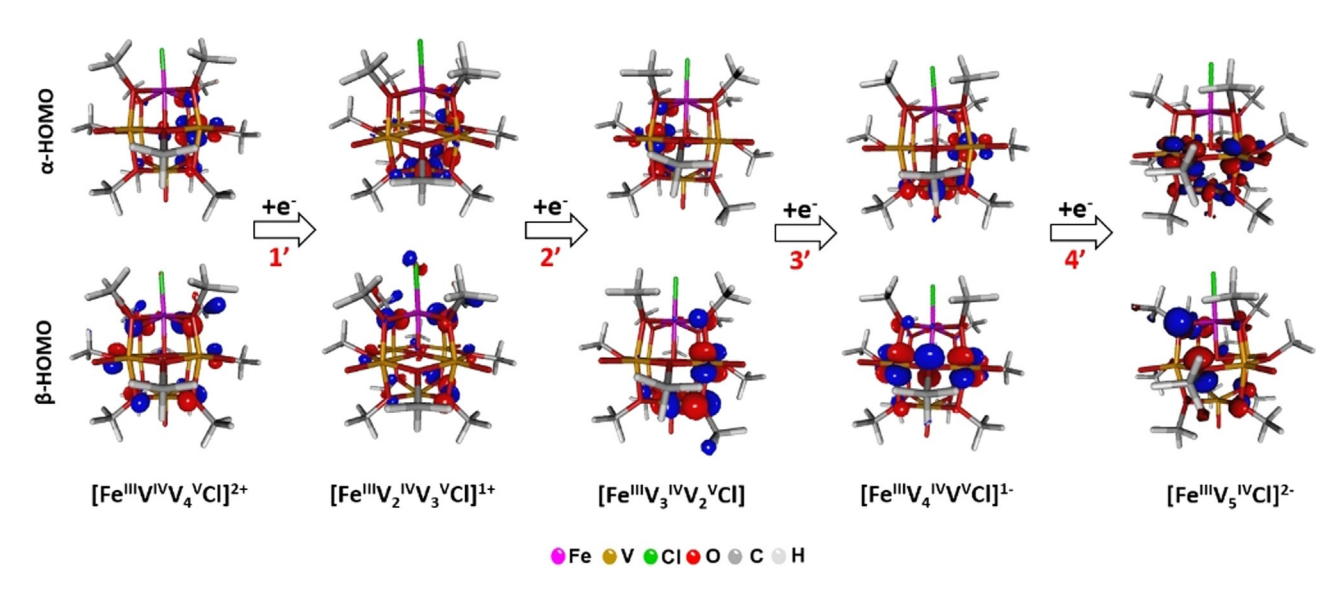


Figure 4. Frontier molecular orbital plots showing the highest occupied molecular orbitals (HOMO) for the complete set of redox-isomers of 1-[V₅FeCI]. Red numbers mark the reduction steps experimentally observed in cyclic voltammetry (Table 1).

into the different behavior observed upon oxidation from the [Fe^{III}V^{IV}₃V^V₂] form. These oxidative processes were selected to be interrogated since calculations were shown to model the E_{1/2} values for these processes better than their reductive counterparts. In particular, we calculated the HOMO energies of the clusters upon oxidation starting from the parent $[V^{IV}_{2}V^{V}_{2}Fe^{III}]$ state. As shown in Figure 5, we observe that for 1-[V₅FeCl] the first and second oxidations are energetically more accessible when compared to the first and second oxidations of 2-[V₅Fe]ClO₄. This suggests that within the accessible solvent window, the first and second oxidation of 1-[V₅FeCl] are energetically possible. In contrast, for 2-[V₅Fe]ClO₄, only the first oxidation is observed, while the second oxidation—while thermodynamically possible—is located outside the solvent stability window. These results are consistent with the increased negative charge provided by the chloride (or cyanate) anion stabilizing the oxidative processes.

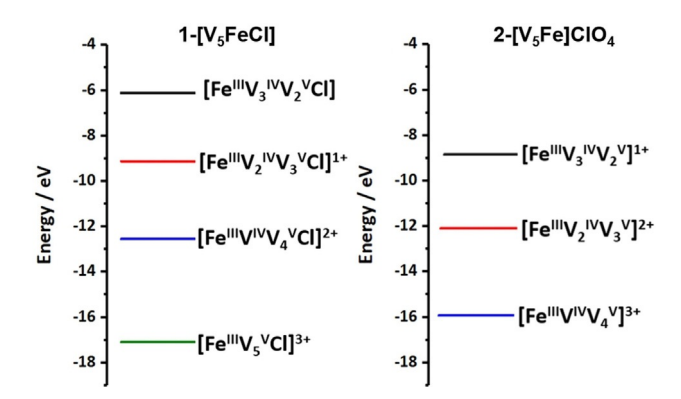


Figure 5. HOMO energies of 1-[V₅FeCl] and 2-[V₅Fe]ClO₄ upon oxidation, showing that the oxidation of $1-[V_5FeCI]$ is energetically less demanding compared with 2-[V₅Fe]ClO₄.

Rationalizing shifts in half-wave potentials in transition metal functionalized POV-alkoxide clusters

Comparing the CV of 1-[V₅FeCl] to other previously reported heterometal-functionalized POV-alkoxide clusters (Figure S22, Table S7), the $E_{1/2}$ values **1-[V₅FeCI]** and the gallium derivative are essentially identical. This is notable, as Ga^{III} has been used as a redox innocent surrogate for Fe^{III} in bioinorganic studies due to their similar charge and ionic radii.[16] The redox profiles of these clusters are anodically shifted from the parent, hexavanadate cluster, $[V_6O_7(OCH_3)_{12}]$, by about 0.10 V and cathodically shifted from the group 4 derivatives, $[V_5O_6(OCH_3)_{12}M(OCH_3)]$ (M = Ti^{IV}, Zr^{IV}, Hf^{IV}), by about 0.40 V.

In an effort to develop a model that rationalizes and predicts the observed shifts in the CV of heterometallic POV-alkoxide clusters, we looked for correlations between quantitative parameters describing physical properties of the heteroions and the $E_{1/2}$ values of the POV-alkoxide compounds. Lewis acidity has been shown to be a good predictor for shifts in the electrochemical profiles of bimetallic^[17] and multi-metallic^[18] systems. Specifically, the aqueous $p\textit{K}_{a}\text{, }p\textit{K}_{a}(H_{2}O)\text{, of the installed}$ heteroion has been used as a measure of the Lewis acidity in order to quantify these effects. Taking inspiration from these studies, the electrochemical potentials of the [V^{IV}₅M]/[V^{IV}₄V^VM] redox event for $[V_5O_6(OCH_3)_{12}MX]$ $(M = Hf^{4+}, Zr^{4+}, Ti^{4+}, X =$ OCH_3^- ; $M = Fe^{3+}$, Ga^{3+} , $X = CI^-$; $M = V^{4+}$, $X = O^{2-}$) clusters, in acetonitrile, were plotted against the $pK_a(M(OH_2)_n)$ of the installed heteroion (Figure 6, Table S7). Similar plots comparing E_{1/2} vs. pK_a (M(OH₂)_n) for the other redox events were analyzed and are reported in the supporting information file (Figure S23, Table S7). Good correlations between the positions of the vanadium-based redox events and the Lewis acidity of the heteroion were observed ($R^2 = 0.79-0.90$). The $E_{1/2}$ values decreased by an average of -150 ± 9 mV per p K_a unit, which is consistent with our previous analysis of redox dependence on Lewis acidity for these Lindqvist POV systems. [12d] Interestingly, the steep-

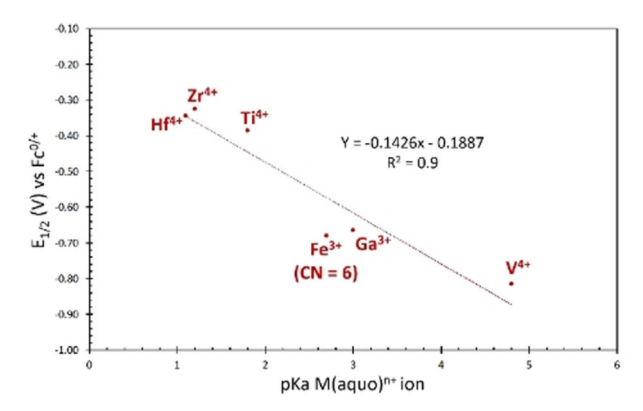


Figure 6. Plot of the half wave potential of the $V^{lv}_{5}M/V^{lv}_{4}V^{V}M$ redox couple $(M=Hf^{4+},Zr^{4+},Ti^{4+},Fe^{3+},Ga^{3+},$ and $V^{4+})$ of POV-alkoxide clusters (acetonitrile, 0.1 M [$nBu_{4}N$][PF₆] as supporting electrolyte, referenced to $Fc^{0/+}$) versus the pKa of the aqueous heteroion (M). CN refers to the coordination number around Fe^{3+} . **2-**[$V_{5}Fe$]CIO₄ (CN = 5) is excluded from this analysis.

ness of the slope steadily increases from about $-140 \, \mathrm{mV/pK_a}$ for the most cathodic $[V^{lv}_5 \mathrm{M}]/[V^{lv}_4 V^{V} \mathrm{M}]$ couple to $-160 \, \mathrm{mV/pK_a}$ for the most anodic $[V^{lv}_2 V^{V}_3 \mathrm{M}]/[V^{lv} V^{V}_4 \mathrm{M}]$ couple. This suggests that the Lewis acidity of the heteroion has a greater influence on the redox properties of the more oxidized species of these clusters. Furthermore, these slopes are significantly steeper than those reported previously for heterometallic systems, specifically bimetallic, Schiff base cobalt (ca. $-50 \, \mathrm{mV/pK_a})^{[17a]}$ and nickel (ca. $-70 \, \mathrm{mV/pK_a})^{[17c]}$ complexes and tetranuclear iron oxide (ca. $-70 \, \mathrm{mV/pK_a})^{[18d]}$ and manganese oxide (ca. $-100 \, \mathrm{mV/pK_a})^{[18b,c]}$ clusters. Thus, for the heterometal-functionalized POV-alkoxide clusters, the electrochemistry of the surrounding vanadium centers appears to be particularly sensitive to the Lewis acceptor capability of the incorporated heteroion.

Notably, iron-functionalized POV-alkoxides with weakly coordinating anions, namely $2\text{-}[V_5\text{Fe}]\text{CIO}_4$ and $2\text{-}[V_5\text{Fe}]\text{OTf}$, deviate substantially from the linear relationship between the Lewis acidity of the installed heteroion established for all other heterometallic, POV-alkoxide clusters reported to date (Figure S24, Table S7). For example, $2\text{-}[V_5\text{Fe}]\text{CIO}_4$ exhibits $E_{1/2}$ values at significantly more reducing potentials (shifted by ca. -0.17 V) compared to that of $1\text{-}[V_5\text{FeCI}]$. This is likely due to the fact that the aqua species used for these pK_a determinations are six-coordinate iron centers, thus rendering these values poor representations of the Lewis acidity of the 5-coordinate iron center.

The differences in the electronic profiles of the 5-coordinate and 6-coordinate iron-functionalized clusters run deeper than the overall shift in the redox profiles of the two clusters. For example, complex $2-[V_5Fe]CIO_4$ supports an additional cathodic event at -1.46 V, which was assigned to a $[V^{V}_5Fe^{|||}]/[V^{|||}V^{V}_4Fe^{|||}]$ couple, that does not occur in $1-[V_5FeCI]$. These results are counter-intuitive, given that, based on the cathodic shift in the CV, $2-[V_5Fe]CIO_4$ is clearly more electron rich as compared to its 6-coordinate congener. Furthermore, only one oxidized species of $2-[V_5Fe]CIO_4$ ($[V^{||}_2V^{||}_3Fe^{||}]^{2+}$) has been observed experimentally, while the CV of $1-[V_5FeCI]$ displayed

two oxidation processes $([V^N_3V^V_2Fe^{III}]/[V^N_2V^V_3Fe^{III}]^{1+}$ and $[V^N_2V^N_3Fe^{III}]^{1+}/[V^NV_4Fe^{III}]^{2+})$. Overall, the ligand environment surrounding the iron influences the electrochemical behavior of these iron-functionalized clusters in a complex manner such that simple electrostatic and Lewis acidity arguments cannot predict. In the cobalt-doped polyoxotitanate cages, $[Ti_4O(OC_2H_5)_{15}CoX]$ and $[Ti_7O_5(OC_2H_5)_{19}CoX]$ ($X = OC_2H_5$ ', F', CI', Br', and I'), the ligand field of cobalt center has a significant effect on the optical band gap of these clusters. Similarly, ligand field effects could also be significant for the open-shell Fe^{III} center in the iron-functionalized, POV-alkoxides reported herein. We still do not fully understand the cause for the differences in the electrochemistry of 1-[V_5FeCI] and 2-[V_5Fe]CIO_4, which is the subject of ongoing investigations by our research team.

Conclusions

Herein, combined experimental and theoretical analyses of the electrochemical features of two iron-polyoxovanadate-alkoxide clusters have been studied, focusing on the changes in electrochemical behavior between five-coordinate and six-coordinate iron sites. Coordination of a chloride to the iron(III) center led to an anodic shift in the redox events and stabilization of an additional oxidative feature in the CV. Both experimental and theoretical studies showed that storage and release of electron density is localized within the vanadate cluster core for 1-[V₅FeCl], which was also seen in previously reported 2-[V₅Fe]ClO₄. Furthermore, changing the geometry of the ferric center from square pyramidal to octahedral upon coordination of the chloride ligand appears to tune these vanadium-based redox events by adjusting the orbital overlap between the iron and the POV metalloligand. Therefore, both the type and the ligand environment of the installed heteroion will be important in selectively designing polyoxovanadate clusters with specific electrochemical properties.

Experimental Section

General Considerations: All manipulations were carried out in the absence of water and oxygen in a UniLab MBraun inert atmosphere glovebox under an atmosphere of dinitrogen. Glassware was oven dried for a minimum of 4 hours and cooled in an evacuated antechamber prior to use in the drybox. Celite 545 (J. T. Baker) was dried in a Schlenk flask for at least 14 hours at 150°C under vacuum prior to use. 3 Å molecular sieves (Fisher Scientific) were activated using the same drying method. All solvents were dried and deoxygenated on a Glass Contour System (Pure Process Technology, LLC) and stored over activated 3 Å molecular sieves. Nitrosonium hexafluorophosphate (NOPF₆, 96%) was purchased from Alfa Aesar and used as received. Tris(4-bromophenyl)ammoniumyl hexachloroantimonate ((N(C₆H₄Br-4)₃)SbCl₆, technical grade) and bis(cyclopentadienyl)cobalt(II) (CoCp₂, 98%) were purchased from Sigma-Aldrich and used as received. Tetrabutylammonium hexafluorophosphate ((nBu₄N)PF₆, 98%) was also purchased from Sigma-Aldrich, recrystallized three times from hot ethanol, and stored under dynamic vacuum in the glovebox prior to use. Potassium graphite $(KC_8),$ $[V_5O_6(OCH_3)_{12}FeCI]$ (1-[V₅FeCl]),



 $[V_5O_6(OCH_3)_{12}Fe]CIO_4$ (2- $[V_5Fe]CIO_4$), and $[V_5O_6(OCH_3)_{12}FeOCN]$ (2- $\textbf{[V}_{5}\textbf{FeOCN]}) were \ prepared \ according \ to \ literature \ precedent.^{\texttt{[12b,d,20]}}$

¹H NMR spectra were recorded on a Bruker DPX-400 MHz spectrometer locked on the signal of deuterated solvents. All chemical shifts were reported relative to the peak of residual ¹H signal in the deuterated solvents. CD₃CN and [D₈]THF were purchased from Cambridge Isotope Laboratories, degassed by three freeze-pumpthaw cycles, and stored over activated 3 Å molecular sieves. Infrared (FT-IR, ATR) spectra of complexes were recorded on a Shimadzu IRAffinity-1 Fourier Transform Infrared spectrophotometer and were reported in wavenumbers (cm⁻¹). Electronic absorption measurements were recorded at room temperature in anhydrous acetonitrile in a sealed 1 cm quartz cuvette with an Agilent Cary 60 UV/ Vis spectrophotometer. A single crystal of 4-CoCp₂[V₅FeCl], was placed on the tip of a thin glass optical fiber (goniometer head) and mounted on a Rigaku XtaLab Synergy-S Dualflex diffractometer equipped with a HyPix-6000HE HPC area detector for data collection at 100.00(10) K. The structure was solved using ShelXT and refined using ShelXL. Elemental analyses were performed on a PerkinElmer 2400 Series II Analyzer at the CENTC Elemental Analysis Facility, University of Rochester.

Cyclic Voltammetry measurements were carried out at room temperature in a nitrogen filled glove box, using a Bio-Logic SP 150 potentiostat/galvanostat and the EC-lab software suite. Cyclic voltammograms were recorded using a glassy carbon working electrode (ø = 3.0 mm) and a Pt wire auxiliary electrode, both purchased from CH Instruments, USA. An Ag/Ag+ non-aqueous reference electrode with 0.01 M AgNO₃ in 0.05 M (nBu₄N)PF₆ in CH₃CN was purchased from Bio-Logic and used as the reference electrode for all cyclic voltammetry measurements. The cyclic voltammograms were collected with 1 mm active species in 0.1 m ([nBu₄N)PF₆ solutions in dry acetonitrile. All redox events were referenced against Fc^{+/0} redox couple.

Synthesis of [V₅O₆(OCH₃)₁₂FeCl]SbCl₆·(THF)_{0.5} (**3-[V₅FeCl]SbCl₆**): In a glovebox, a 20 mL scintillation vial was charged with 1-[V₅FeCl] (97 mg, 0.12 mmol, 1.0 equiv) and 10 mL acetonitrile. Solid $(N(C_6H_4Br-4)_3)SbCl_6$ (95 mg, 0.12 mmol, 1.0 equiv) was then added in small portions. The cloudy, dark green mixture was stirred at room temperature for thirty minutes. The reaction mixture was filtered over a bed of Celite (1.0 cm) on a medium-porosity frit, and the volatiles were removed under reduced pressure. The resulting dark green solid was triturated with toluene (10 mL x 5) and diethyl ether (10 mL). The solid was extracted with acetonitrile (2 mL x 4) and filtered over a bed of Celite (1.0 cm) on a medium-porosity frit. The dark green solution was concentrated to half the original volume and was allowed to crystallize at -30 °C overnight. Complex 3-[V₅FeCl]SbCl₆ was isolated as a shiny, green solid (48 mg, 0.04 mmol, 35% yield based on $1-[V_5FeCl]$). ¹H NMR (400 MHz, CD₃CN): $\delta = 14.59$ (fwhh = 260 Hz), 12.71 (fwhh = 400 Hz). FT-IR (ATR, cm⁻¹): 984 ($V = O_t$). UV/Vis [CH₃CN; λ , nm (ε , 1×10³ m⁻¹ cm⁻¹)]: 316 (9.92), 382 (8.01), 992 (0.66). Elemental analysis calculated for $C_{12}H_{36}O_{18}V_5FeSbCl_7^{*1}/_2$ THF (%) (MW = 1184.92 g mol⁻¹): C, 14.19; H, 3.06; Found (%): C, 14.39; H, 2.83.

Synthesis of $K[V_5O_6(OCH_3)_{12}FeCl]\cdot(MeCN)_{1.25}(THF)_{0.25}$ (4- $K[V_5FeCl]$): In a glovebox, a 20 mL scintillation vial was charged with 1-[V₅FeCl] (199 mg, 0.25 mmol, 1.0 equiv) and 18 mL tetrahydrofuran. Solid KC₈ (32 mg, 0.24 mmol, 1.0 equiv) was then added in small portions. The cloudy, dark green mixture was stirred at room temperature for an hour. The reaction mixture was filtered over a bed of Celite (1.0 cm) on a medium-porosity frit, and the volatiles were removed under reduced pressure. The resulting dark green solid was triturated with toluene (10 mL x 3), dichloromethane (10 mL x 3), and diethyl ether (10 mL x 3). The solid was extracted with acetonitrile, filtered over a bed of Celite (1.0 cm) on a medium-porosity frit, and the volatiles were removed under reduced pressure, affording complex 4-K[V₅FeCl] as a dark green solid (181 mg, 0.21 mmol, 87% yield based on 1-[V₅FeCl]). ¹H NMR (400 MHz, CD₃CN): $\delta = 23.76$ (fwhh = 396 Hz), 18.09 (fwhh = 620 Hz), 5.66 (fwhh = 28 Hz). FT-IR (ATR, cm⁻¹): 1020 (O_b-CH₃), 957 ($V = O_t$). Elemental analysis calculated for $C_{12}H_{36}O_{18}V_5FeKCl^{\bullet}\ 1^{1}/_{\!\!4}$ MeCN $^{1}/_{\!\!4}$ THF (%) (MW = 992.85 g mol $^{-1}$): C, 20.17; H, 4.56; N, 1.90; Found (%): C, 20.27; H, 4.44; N, 2.12.

Synthesis of $CoCp_2[V_5O_6(OCH_3)_{12}FeCl]\cdot (DCM)_{0.5}$ (4-CoCp₂[V₅FeCl]): In a glovebox, a 20 mL scintillation vial was charged with 1-[V₅FeCl] (116 mg, 0.14 mmol, 1.0 equiv) and 12 mL tetrahydrofuran. Solid CoCp₂ (32 mg, 0.17 mmol, 1.2 equiv) was then added in small portions. The cloudy, dark green mixture was stirred at room temperature for an hour. The reaction mixture was filtered over a bed of Celite (1.0 cm) on a medium-porosity frit, and the volatiles were removed under reduced pressure. The resulting dark green solid was triturated with toluene (10 mL x 3) and diethyl ether (10 mL x 3). The solid was extracted with dichloromethane, filtered over a bed of Celite (1.0 cm) on a medium-porosity frit, and the volatiles were removed under reduced pressure, affording complex 4- $\textbf{CoCp}_{2}[\textbf{V}_{5}\textbf{FeCI}]$ as a dark green solid (103 mg, 0.10 mmol, 73 % yield based on 1-[V₅FeCl]). Crystals suitable for X-ray analysis were grown from slow diffusion of pentane into a saturated solution of **4-CoCp**₂[**V**₅**FeCl**] in tetrahydrofuran. ¹H NMR (400 MHz, CD₃CN): δ = 23.76 (fwhh = 396 Hz), 18.09 (fwhh = 620 Hz), 5.66 (fwhh = 28 Hz). FT-IR (ATR, cm⁻¹): 1024 (O_b-CH₃), 959 ($V = O_t$). UV/Vis [CH₃CN; λ , nm $(\varepsilon, 1 \times 10^3 \,\mathrm{M}^{-1} \,\mathrm{cm}^{-1})$]: 300 (9.71), 382 (3.65), 992 (0.55). Elemental analysis calculated for $C_{22}H_{46}O_{18}V_5FeCoCl^{-1}/_2$ DCM (%) (MW= 1045.99 g mol⁻¹): C, 25.84; H, 4.53; Found (%): C, 25.89; H, 4.23.

Synthesis of $(CoCp_2)_2[V_5O_6(OCH_3)_{12}FeCl]\cdot (DCM)_{0.5}$ (5-(CoCp₂)₂-[V₅FeCl]): In a glovebox, a 20 mL scintillation vial was charged with 1-[V₅FeCl] (143 mg, 0.18 mmol, 1.0 equiv) and 16 mL tetrahydrofuran. Solid CoCp₂ (66 mg, 0.35 mmol, 2.0 equiv) was then added in small portions. The teal slurry was stirred at room temperature for an hour. The precipitate was collected over a bed of Celite (1.0 cm) on a medium-porosity frit and triturated with fresh tetrahydrofuran (10 mL x 3). The remaining teal solid was extracted with acetonitrile (2 mL x 3), and the volatiles were removed under reduced pressure. The resulting solid was triturated with dichloromethane (10 mL x 3), affording complex 5-(CoCp₂)₂[V_5 FeCl] as a teal solid (88 mg, 0.07 mmol, 42% yield based on 1-[V₅FeCl]). Crystals suitable for X-ray analysis were grown from slow diffusion of diethyl ether into a saturated solution of 5-(CoCp₂)₂[V₅FeCl] in dichloromethane. $^{1}\text{H NMR}$ (400 MHz, CD3CN): $\delta\!=\!24.91$, 21.88, 5.69 (92 Hz). FT-IR (ATR, cm⁻¹): 1043 (O_b -CH₃), 941 ($V = O_t$). UV/Vis [CH₃CN; λ , nm $(\varepsilon, 1 \times 10^3 \,\mathrm{m}^{-1} \,\mathrm{cm}^{-1})$]: 296 (7.16), 598 (0.24). Elemental analysis calculated for $C_{32}H_{56}O_{18}V_5FeCo_2Cl \cdot \frac{1}{2}$ DCM (%) (MW = 1235.12 g mol⁻¹): C, 31.61; H, 4.65; Found (%): C, 31.62; H, 4.38.

Acknowledgements

This research was funded by the National Science Foundation through grant CHE-1653195 (R. L. M., B. E. P. and E. M. M.). R. L. M., B. E. P., and E. M. M. also acknowledge financial support from the University of Rochester. M.H.A. and C.S. gratefully acknowledge financial support by the Deutsche Forschungsgemeinschaft DFG (EXC-2154 "PoLiS", STR1164/12), Ulm University and the Helmholtz-Gemeinschaft. M.H.A. gratefully acknowledges the Federal State of Baden-Württemberg for a Margarete-von-Wrangell Fellowship.



Conflict of interest

The authors declare no conflict of interest.

Keywords: coordination chemistry \cdot electrochemistry \cdot metal oxide \cdot polyoxometalate \cdot self-assembly

- [1] a) S. Wang, W. Sun, Q. Hu, H. Yan, Y. Zeng, Bioorg. Med. Chem. Lett. 2017, 27, 2357 – 2359; b) D.-D. Zhang, Z.-Y. Guo, P.-F. Guo, X. Hu, X.-W. Chen, J.-H. Wang, ACS Appl. Mater. Interfaces 2018, 10, 21876 – 21882.
- [2] a) E. Coronado, C. J. Gómez-García, Chem. Rev. 1998, 98, 273 296; b) D.-L. Long, E. Burkholder, L. Cronin, Chem. Soc. Rev. 2007, 36, 105 121;
 c) Y.-F. Song, R. Tsunashima, Chem. Soc. Rev. 2012, 41, 7384 7402; d) A. Proust, B. Matt, R. Villanneau, G. Guillemot, P. Gouzerh, G. Izzet, Chem. Soc. Rev. 2012, 41, 7605 7622.
- [3] a) A. Müller, F. Peters, M. T. Pope, D. Gatteschi, Chem. Rev. 1998, 98, 239–272; b) J. M. Clemente-Juan, E. Coronado, A. Gaita-Ariño, Chem. Soc. Rev. 2012, 41, 7464–7478.
- [4] a) X. Zhao, S. Zhang, J. Yan, L. Li, G. Wu, W. Shi, G. Yang, N. Guan, P. Cheng, *Inorg. Chem.* 2018, 57, 5030-5037; b) I. A. Weinstock, R. E. Schreiber, R. Neumann, *Chem. Rev.* 2018, 118, 2680-2717; c) S.-S. Wang, G.-Y. Yang, *Chem. Rev.* 2015, 115, 4893-4962.
- [5] a) M. Genovese, K. Lian, Curr. Opin. Solid St. Mater. Sci. 2015, 19, 126–137; b) Y. Ji, L. Huang, J. Hu, C. Streb, Y.-F. Song, Energy Environ. Sci. 2015, 8, 776–789.
- [6] M. Sadakane, E. Steckhan, Chem. Rev. 1998, 98, 219-238.
- [7] a) H. D. Pratt, W. R. Pratt, X. Fang, N. S. Hudak, T. M. Anderson, *Electrochim. Acta* 2014, *138*, 210–214; b) H. D. Pratt, N. S. Hudak, X. Fang, T. M. Anderson, *J. Power Sources* 2013, *236*, 259–264; c) L. E. VanGelder, E. M. Matson, *J. Mater. Chem. A* 2018, *6*, 13874–13882; d) L. E. VanGelder, A. M. Kosswattaarachchi, P. L. Forrestel, T. R. Cook, E. M. Matson, *Chem. Sci.* 2018, *9*, 1692–1699; e) L. E. VanGelder, B. E. Petel, O. Nachtigall, G. Martinez, W. W. Brennessel, E. M. Matson, *ChemSusChem* 2018, *11*, 4139–4149
- [8] J.-J. J. Chen, M. A. Barteau, Indust. Eng. Chem. Res. 2016, 55, 9857 9864.
- [9] Y. Hayashi, Coord. Chem. Rev. 2011, 255, 2270 2280.
- [10] a) J. Tucher, L. C. Nye, I. Ivanovic-Burmazovic, A. Notarnicola, C. Streb, Chem. Eur. J. 2012, 18, 10949-10953; b) J. Forster, B. Rösner, M. M. Khusniyarov, C. Streb, Chem. Commun. 2011, 47, 3114-3116; c) K. Kastner, J. Forster, H. Ida, G. N. Newton, H. Oshio, C. Streb, Chem. Eur. J. 2015, 21, 7686-7689; d) C. Aronica, G. Chastanet, E. Zueva, S. A. Borshch, J. M. Clemente-Juan, D. Luneau, J. Am. Chem. Soc. 2008, 130, 2365-2371; e) J. M. Cameron, G. N. Newton, C. Busche, D.-L. Long, H. Oshio, L. Cronin, Chem. Commun. 2013, 49, 3395-3397; f) M. H. Anjass, K. Kastner, F. Nägele, M. Ringenberg, J. F. Boas, J. Zhang, A. M. Bond, T. Jacob, C. Streb, Angew. Chem. Int. Ed. 2017, 56, 14749-14752; Angew. Chem. 2017, 129, 14944-14947.

- [11] a) J. Spandl, C. Daniel, I. Brüdgam, H. Hartl, Angew. Chem. Int. Ed. 2003, 42, 1163–1166; Angew. Chem. 2003, 115, 1195–1198; b) C. Daniel, H. Hartl, J. Am. Chem. Soc. 2005, 127, 13978–13987; c) C. Daniel, H. Hartl, J. Am. Chem. Soc. 2009, 131, 5101–5114.
- [12] a) F. Li, L. E. VanGelder, W. W. Brennessel, E. M. Matson, *Inorg. Chem.* 2016, 55, 7332–7334; b) F. Li, S. H. Carpenter, R. F. Higgins, M. G. Hitt, W. W. Brennessel, M. G. Ferrier, S. K. Cary, J. S. Lezama-Pacheco, J. T. Wright, B. W. Stein, M. P. Shores, M. L. Neidig, S. A. Kozimor, E. M. Matson, *Inorg. Chem.* 2017, 56, 7065–7080; c) L. E. VanGelder, W. W. Brennessel, E. M. Matson, *Dalton Trans.* 2018, 47, 3698–3704; d) R. L. Meyer, W. W. Brennessel, E. M. Matson, *Polyhedron* 2018, 156, 303–311.
- [13] N. G. Connelly, W. E. Geiger, Chem. Rev. 1996, 96, 877 910.
- [14] L. E. VanGelder, P. L. Forrestel, W. W. Brennessel, E. M. Matson, Chem. Commun. 2018, 54, 6839 – 6842.
- [15] a) K. Yu. Monakhov, O. Linnenberg, P. Kozłowski, J. van Leusen, C. Besson, T. Secker, A. Ellern, X. López, J. M. Poblet, P. Kögerler, Chem. Eur. J. 2015, 21, 2387–2397; b) S. Herrmann, N. Aydemir, F. Nägele, D. Fantauzzi, T. Jacob, J. Travas-Sejdic, C. Streb, Adv. Funct. Mater. 2017, 27, 1700881; c) A. D. Bochevarov, E. Harder, T. F. Hughes, J. R. Greenwood, D. A. Braden, D. M. Philipp, D. Rinaldo, M. D. Halls, J. Zhang, R. A. Friesner, Int. J. Quant. Chem. 2013, 113, 2110–2142.
- [16] a) Y. Kaneko, M. Thoendel, O. Olakanmi, B. E. Britigan, P. K. Singh, J. Clin. Invest. 2007, 117, 877 888; b) C. R. Chitambar, M. M. Al-Gizawiy, H. S. Alhajala, K. R. Pechman, J. P. Wereley, R. Wujek, P. A. Clark, J. S. Kuo, W. E. Antholine, K. M. Schmainda, Mol. Cancer Therap. 2018, 17, 1240 1250; c) C. R. Chitambar, Pharmacological Research 2017, 115, 56 64; d) C. R. Chitambar, Biochim. Biophys. Acta Mol. Cell Res. 2016, 1863, 2044 2053; e) R. Shannon, Acta Crystallogr. Sect. A 1976, 32, 751 767.
- [17] a) A. H. Reath, J. W. Ziller, C. Tsay, A. J. Ryan, J. Y. Yang, *Inorg. Chem.* 2017, 56, 3713–3718; b) T. Chantarojsiri, J. W. Ziller, J. Y. Yang, *Chem. Sci.* 2018, 9, 2567–2574; c) A. Kumar, D. Lionetti, V. W. Day, J. D. Blakemore, *Chem. Eur. J.* 2018, 24, 141–149.
- [18] a) V. Krewald, F. Neese, D. A. Pantazis, Phys. Chem. Chem. Phys. 2016, 18, 10739-10750; b) E. Y. Tsui, T. Agapie, Proc. Natl. Acad. Sci. USA 2013, 110, 10084-10088; c) E. Y. Tsui, R. Tran, J. Yano, T. Agapie, Nat. Chem. 2013, 5, 293-299; d) D. E. Herbert, D. Lionetti, J. Rittle, T. Agapie, J. Am. Chem. Soc. 2013, 135, 19075-19078; e) P.-H. Lin, M. K. Takase, T. Agapie, Inora. Chem. 2015, 54, 59-64.
- [19] S. Hanf, P. D. Matthews, N. Lo, H.-K. Luo, D. S. Wright, *Dalton Trans*. 2017, 46, 578–585.
- [20] I. S. Weitz, M. Rabinovitz, J. Chem. Soc. Perkin Trans. 1993, 117 120.

Manuscript received: December 12, 2019 Revised manuscript received: March 13, 2020 Accepted manuscript online: March 20, 2020 Version of record online: June 25, 2020

www.chemeurj.org